Experiments and Modeling of Autoignition of Methyl Valerate at Low to Intermediate Temperatures and Elevated Pressures in a Rapid Compression Machine

Bryan W. Weber[a,*], Justin Bunnell[a], Kamal Kumar[b], Chih-Jen Sung[a]

[a]*Department of Mechanical Engineering, University of Connecticut, Storrs, CT, USA*
[b]*Department of Mechanical Engineering, University of Idaho, Moscow, ID, USA*

Abstract

Methyl valerate ($C_6H_{12}O_2$, methyl pentanoate) is a methyl ester and a relevant surrogate component for biodiesel. In this work, we present ignition delays of methyl valerate measured using a rapid compression machine at a range of engine-relevant temperature, pressure, and equivalence ratio conditions. The conditions we have studied include equivalence ratios from 0.25 to 2.0, temperatures between 680 K and 1050 K, and pressures of 15 bar and 30 bar. The ignition delay data demonstrate a negative temperature coefficient region in the temperature range of 720 K–800 K for both $\phi = 2.0$, 15 bar and $\phi = 1.0$, 30 bar, with two-stage ignition apparent over the narrower temperature ranges of 720 K–760 K for the lower pressure and 740 K–760 K at the higher pressure. In addition, the experimental ignition delay data are compared with simulations using an existing chemical kinetic model from the literature. The simulations with the literature model under-predict the data by factors between 2 and 10 over the entire range of the experimental data. In addition, a new chemical kinetic model is developed using the Reaction Mechanism Generator (RMG) software. The agreement between the experimental data and the RMG model is also not satisfactory. To help determine the possible reasons for the disagreement, a path analysis of both models is completed. It is found that improvements to both the reaction pathways and thermodynamic properties is required. Further

*Corresponding Author: bryan.weber@uconn.edu

directions for future improvement of the methyl valerate model are discussed.

1. Introduction

For transportation applications, biodiesel is an important constituent in improving environmental friendliness of fuels. This is due to its renewability when produced from sustainable agricultural crops and its ability to reduce emissions relative to conventionally fueled engines [1]. Biodiesel typically consists of long-chain methyl ester molecules, with typical compositions of C_{14} to C_{20} [1]. Recognizing that the large molecular size of the methyl esters within biodiesel fuel makes creating and using detailed chemical kinetic mechanisms challenging [2], it is desired to study their combustion chemistry by studying simpler methyl ester molecules.

A recent review paper summarizes the work on methyl esters relevant to biodiesel combustion [3]; the following summary focuses on ignition delay measurements, since these are the focus of this paper. Autoignition of methyl butanoate (MB, $C_5H_{10}O_2$) has been well-studied in both shock tube and rapid compression machine experiments [4, 5, 6, 7, 8, 9, 10]. The prevalence of MB data in the literature is largely due to the early identification of MB as a potential surrogate fuel for biodiesel [11]. However, the experiments have shown that MB may not be an appropriate surrogate for biodiesel, due to its lack of negative temperature coefficient (NTC) behavior, a requirement for a suitable biodiesel surrogate [3].

Larger methyl esters such as methyl valerate (MV, $C_6H_{12}O_2$, methyl pentanoate) have also been studied as possible biodiesel surrogates. Hadj-Ali et al. [9] used a rapid compression machine (RCM) to study the autoignition of several methyl esters including MV. Although MV exhibited two-stage ignition in this study, little additional research has been done on its oxidation. Korobeinichev et al. [12] studied MV in premixed laminar flames and extended a detailed

high temperature chemical kinetic model to include MV and methyl hexanoate. Dmitriev et al. [13] added MV to n-heptane/toluene fuel blends to determine the resulting intermediate species in premixed flames using a flat burner at 1 atm and an equivalence ratio of 1.75. The addition of MV helped reduce soot forming intermediates including benzene, cyclopentadienyl, acetylene, propargyl, and vinylacetylene [13]. Hayes and Burgess [14] computationally examined the peroxy radical isomerization reactions for MV to better understand the low temperature reaction pathways. Finally, Diévart et al. [15] used diffusion flames in the counterflow configuration to determine extinction limits for a number of methyl esters, including MV, and validated a detailed kinetic model with the experimental data.

This work provides additional data for the autoignition of MV. Data is collected in a RCM under engine relevant conditions spanning from 15 bar to 30 bar, equivalence ratios from 0.25 to 2.0, and temperatures from 682 K to 1048 K. The NTC region of MV is mapped out to provide additional information on the fidelity of using MV as a biodiesel surrogate.

2. Experimental Methods

The RCM used in this study is a single piston arrangement and is pneumatically driven and hydraulically stopped. The device has been described in detail previously [16] and will be described here briefly for reference. The end of compression (EOC) temperature and pressure (T_C and P_C respectively), are independently changed by varying the overall compression ratio, initial pressure (P_0), initial temperature (T_0), and specific heat ratio of the experiments. The piston in the reaction chamber is machined with a specially designed crevice to suppress the roll-up vortex effect and promote homogeneous conditions in the reactor during and after compression [17].

The primary diagnostic on the RCM is the in-cylinder pressure measured by a Kistler 6125C dynamic transducer that is compensated for thermal shock. The transducer is coupled to a Kistler 5010B charge amplifier. The voltage output

⁵⁶ of the charge amplifier is recorded by a National Instruments 9125 analog input
⁵⁷ device connected to a cDAQ 9178 chassis. The voltage is sampled at a rate
⁵⁸ of either 50 kHz or 100 kHz by a LabView VI and processed by a Python
⁵⁹ package called UConnRCMPy [18]. Version 3.0.0 of UConnRCMPy [19], 3.6.1
⁶⁰ of Python, 2.3.0 of Cantera [20], 1.13 of NumPy [21], 0.19.0 of SciPy [22], and
⁶¹ 2.0.1 of Matplotlib [23] were used in the analysis in this paper.

⁶² The compression stroke of the RCM brings the fuel/oxidizer mixture to the
⁶³ EOC conditions, and for suitable thermodynamic states, the mixture will ignite
⁶⁴ after a delay period. The definitions of the ignition delays are shown in Fig. 1.
⁶⁵ The time of the EOC is defined as the maximum of the pressure trace prior to
⁶⁶ the start of ignition and the ignition delays are defined as the time from the EOC
⁶⁷ until local maxima in the first time derivative of the pressure. Each experimental
⁶⁸ condition is repeated at least five times to ensure repeatability of the data. As
⁶⁹ there is some random scatter present in the data, the standard deviation (σ) of
⁷⁰ the ignition delays from the runs at a given condition is computed. In all cases,
⁷¹ σ is less than 10 % of the mean value of the overall ignition delay.

⁷²

4
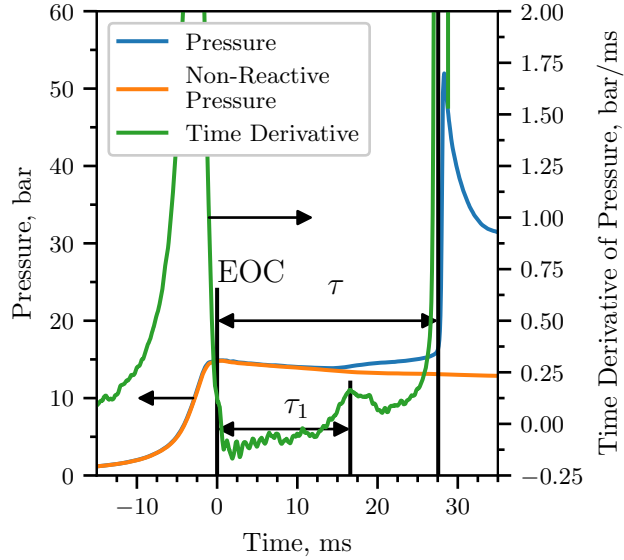
Figure 1: Definition of the ignition delays used in this work. The experiment in this figure was conducted for a $\phi = 2.0$ mixture with $\mathrm{Ar}/(\mathrm{N}_2 + \mathrm{AR}) = 0.5$, $P_0 = 0.7806\,\mathrm{bar}$, $T_0 = 373\,\mathrm{K}$, $P_C = 14.92\,\mathrm{bar}$, $T_C = 720\,\mathrm{K}$, $\tau = (27.56 \pm 0.89)\,\mathrm{ms}$, $\tau_1 = (16.60 \pm 0.46)\,\mathrm{ms}$.

In addition to the reactive experiments, non-reactive experiments are conducted to determine the influence of machine-specific behavior on the experimental conditions and permit the calculation of the EOC temperature via the isentropic relations between pressure and temperature [24]. The EOC temperature is calculated by the procedure described in Section 3.

The mixtures considered in this study are shown in Table 1. Four equivalence ratios of MV in "air" are considered. The ratio of $\mathrm{Ar} : \mathrm{N}_2$ in the oxidizer is varied to adjust the temperatures reached at the EOC for a given mixture. Two P_C conditions are studied in this work, 15 bar and 30 bar, representing engine-relevant conditions. For the $\phi = 2.0$ condition, only $P_C = 15\,\mathrm{bar}$ is considered because we could not achieve T_C values low enough that the ignition was long enough to be measured in our apparatus (the typical lower limit of ignition delay on the present RCM is approximately 5 ms).

Mixtures are prepared in stainless steel mixing tanks, 17 L and 15 L in size. The proportions of reactants in the mixture are determined by specifying the absolute mass of the fuel, the equivalence ratio (ϕ), and the ratio of $\mathrm{Ar} : \mathrm{N}_2$ in the oxidizer. Mixtures are made by first vacuuming the mixing tanks to an ultimate pressure less than 5 torr. Since MV is a liquid with a relatively small vapor pressure at room temperature and pressure, it is measured gravimetrically to within 0.01 g of the specified value. The fuel is injected into the mixing tank through a septum. Proportions of O_2, Ar, and N_2 are added manometrically at room temperature and the total pressure is measured by an Omega Engineering MMA100V10T2D0T4A6 type static pressure transducer. The same transducer is used to measure the pressure of the reactants prior to an experiment.

Table 1: Mixtures considered in this work

| ϕ	Mole Fraction (purity)				Ar/(N$_2$ + Ar)
	MV (100 %)	O$_2$ (99.994 %)	Ar (99.999 %)	N$_2$ (99.999 %)	
0.25	0.0065	0.2087	0.7848	0.0000	1.0
0.5	0.0130	0.2074	0.7798	0.0000	1.0
1.0	0.0256	0.2047	0.7697	0.0000	1.0
1.0	0.0256	0.2047	0.3849	0.3848	0.5
2.0	0.0499	0.1996	0.0000	0.7505	0.0
2.0	0.0499	0.1996	0.3752	0.3753	0.5

The RCM is equipped with heaters to control the initial temperature of the mixture. After filling in the components to the mixing tanks, the heaters are switched on and the system is allowed 1.5 h to come to steady state. The mixing tanks are also equipped with magnetic stir bars so the reactants are well mixed for the duration of the experiments.

The initial temperature is chosen such that the saturated vapor pressure (P_{sat}) of the fuel at the initial temperature is at least twice the partial pressure of the fuel in the mixing tank. The Antoine equation

$$\log_{10} P_{\text{sat}} = A - \frac{B}{T - C} \tag{1}$$

is used to model the saturated vapor pressure of MV as a function of temperature, where A, B, and C are substance-specific coefficients. Coefficients for Eq. (1) are given in the literature by Ortega et al. [25], Camacho et al. [26], and Stephenson et al. [27]. Unfortunately, the values of the coefficients are different among all three authors and, more importantly, the temperature ranges provided in those three fits do not cover the entire range of interest for this study. Therefore, coefficients for use in Eq. (1) are determined in this work by least squares fitting of the data of Ortega et al. [25], van Genderen et al. [28], and Verevkin and Emel'yanenko [29] using the `curve_fit()` function of SciPy [22] version 0.19.0. Figure 2 shows that the coefficients fit with this procedure give

good agreement with the experimental data; values for the coefficients computed in this work and in the literature works are given in Table 2. The data used to calculate the coefficients are provided in the Supplementary Material.
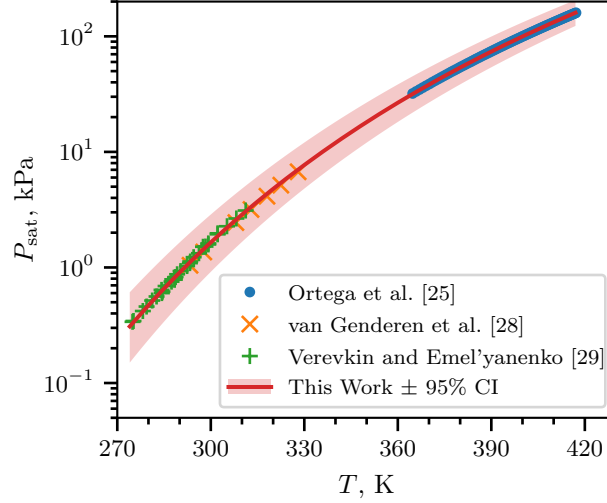
Figure 2: Saturated vapor pressure of MV as a function of temperature, plotted using the Antoine equation, Eq. (1), with $A = 6.4030$, $B = 1528.69$, and $C = 52.881$.

Table 2: Antoine Equation coefficients computed in this work and from the literature. The 2σ confidence interval is estimated by taking the square root of the diagonals of the covariance matrix returned from `curve_fit()`

	A	B	C	$T_{\min}$, K	$T_{\max}$, K
This Work	6.4030	1528.69	52.881	274.9	417.18
2σ Confidence Interval	0.0919	53.47	4.934	—	—
Ortega et al. [25]	6.23175	1429.00	62.30	364.75	417.18
Camacho et al. [26]	5.9644	1281.06	75.94	281	547
Stephenson et al. [27]	6.62646	1658.4	42.09	297	411

7

3. Computational Methods

3.1. RCM Modeling

The Python 3.6 interface of Cantera [20] version 2.3.0 is used for all simulations in this work. Detailed descriptions of the use of Cantera for these simulations can be found in the work of Weber and Sung [18] and Dames et al. [30]; a brief overview is given here. As mentioned in Section 2, non-reactive experiments are conducted to characterize the machine-specific effects on the experimental conditions in the RCM. This pressure trace is combined with the reactive pressure trace and used to compute a volume trace by assuming that the reactants undergo a reversible, adiabatic, constant composition (i.e., isentropic) compression during the compression stroke and an isentropic expansion after the EOC. The volume trace is applied to a simulation conducted in an `IdealGasReactor` in Cantera [20] using the CVODES solver from the SUNDIALS suite [31]. The ignition delay from the simulations is defined in the same manner as in the experiments. The time derivative of the pressure in the simulations is computed by second order Lagrange polynomials, as discussed by Chapra and Canale [32].

To the best of our knowledge, there are three mechanisms for MV combustion available in the literature. The first two, by [12] and [13], were developed to simulate flames, and do not include the low-temperature chemistry necessary to simulate the conditions in these experiments. The third model was developed by [15] and includes low-temperature chemistry of MV, although it was only validated by comparison with flame extinction limits. In converting this mechanism for use in Cantera, we found that there were many species in the thermodynamic database with multiple data entries. For most of these species the thermodynamic data is identical. However, some species are not exact duplicates. For these species, it is not clear from the thermodynamic database file which data set should be preferred. Since Cantera (and CHEMKIN) choose the first instance of a duplicate species to be used, we retained the first entry for all duplicated species. The detailed [15] model includes 1105 species and 7141

8

reactions, and the CHEMKIN and Cantera formatted input files are available in the Supplementary Material.

3.2. Reaction Mechanism Generator

In addition to using a mechanism from the literature, we investigate the use of an automatic mechanism generator, the open-source Reaction Mechanism Generator (RMG) [33] version 2.1.0. The Python version of RMG is used, which requires Python 2.7, and version 2.1.0 of the RMG database is used. The final RMG model contains 427 species and 13640 reactions. Note that the number of species is much lower than the Diévart et al. [15] model because the RMG model focuses on only one fuel (MV), but the number of reactions is substantially higher. The input file used to generate the model is available in the Supplementary Material.

4. Experimental Results

4.1. Ignition Delays

Figure 3 shows the ignition delay results measured in this study. Filled markers denote the overall ignition delay and hollow markers indicate the first-stage ignition delay. Vertical error bars are drawn on the symbols to represent the uncertainty in the ignition delay; for many of the experiments, the uncertainty is approximately the same size as the data point, so the error bar is hidden. Horizontal error bars are shown on the first and last points of each equivalence ratio indicating the estimated uncertainty in the EOC temperature of $\pm 1\%$ [34]. Fig. 3a shows the results for a compressed pressure of 15 bar, while Fig. 3b shows the results for a compressed pressure of 30 bar. Note that $\phi = 2.0$ results were not collected for 30 bar, so there are no red data points in Fig. 3b. All the data are available in comma-separated value files and ChemKED-format [35] files in the Supplementary Material.

It can be seen from Fig. 3 that the ignition delays for the $\phi = 0.25$ and 0.5 mixtures do not show an NTC region of the ignition delay for both of the

9

pressures studied in this work. However, the $\phi = 1.0$ mixture shows an NTC region at $P_C = 30$ bar between approximately 720 K and 800 K, with measured first-stage ignition delays at 733 K and 757 K. In addition, the $\phi = 2.0$ mixture shows an NTC region of ignition delay at 15 bar from approximately 720 K to 780 K, with measured first-stage ignition delays between 720 K and 750 K.
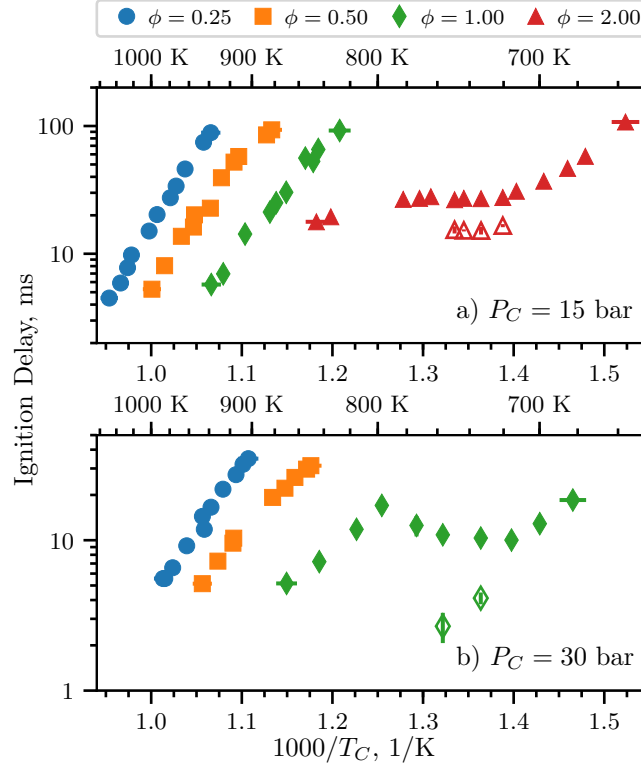
Figure 3: Ignition delays of MV as a function of inverse temperature. Filled points are the overall ignition delays and hollow points are the first stage ignition delays. a) 15 bar. b) 30 bar

Hadj-Ali et al. [9] also observed two-stage ignition of MV in stoichiometric mixtures, stating that "[m]ethyl pentanoate... was more reactive [than methyl butanoate] with a limit below which autoignition no longer occurs observed at $T_c = 670$ K and $P_c = 11.4$ bar. At this temperature, the autoignition occurred in two stages with a clearly identified cool flame event."[9] However, we do not find two stage ignition for the similar pressure of $P_C = 15$ bar in this study. We note that the stated temperature of the experiment from the work of Hadj-

Ali et al. [9] (670 K) is much lower than the lowest temperature we considered in this work at 15 bar, $\phi = 1.0$ (828 K). We did not conduct experiments at lower temperatures because the work of Mittal and Sung [17] showed that the temperature field in the RCM reaction chamber was uniform for approximately 100 ms after the EOC, and our measured ignition delay at 15 bar, $\phi = 1.0$, and 828 K is 92.14 ms.

However, we note NTC behavior of the ignition delay and two-stage ignition at the higher pressure of 30 bar, and at higher temperatures than those reported for two-stage ignition in the study of Hadj-Ali et al. [9]. The trend of NTC behavior shifting to higher temperatures with increasing pressure can be seen in other classes of fuels. Kukkadapu et al. [36] found a similar trend in gasoline composed of iso-alkanes, n-alkanes, cyclo-alkanes, aromatics, and olefins. Kukkadapu et al. [36] attributed the NTC shift to the reactions between the hydroperoxyalkyl radical (QOOH) and O_2 becoming more dominant than the unimolecular decomposition of QOOH at higher pressures. Similar trends could occur for the hydroperoxyalkyl radicals of MV.

To further understand the effect of the methyl ester functional group on the NTC region of ignition delay, we compare with the alkane and alcohol with 5-carbon alkyl chains, n-pentane and n-pentanol. n-Pentane and MV have the same fuel mole percentage for stoichiometric mixtures in air (2.56 %), while n-pentanol has a fuel mole percentage of 2.72 % for stoichiometric conditions. Ribaucour et al. [37] and Bugler et al. [38] found the NTC region for n-pentane to be between 760 K and 910 K at pressures near 10 atm. As we will compare with our MV data at 30 bar, we note that increasing the pressure tends to shift the NTC to higher temperatures, as mentioned previously [36]. Heufer et al. [39] found NTC behavior for n-pentanol in the range of 770 K to 900 K at 30 bar. In this study, we find the NTC window for MV at 30 bar to be between 720 K and 800 K. Therefore, it appears that the methyl ester functional group shifts the NTC range to lower temperature as compared to alkanes and alcohols with similar alkyl chain lengths. This result was also noted by Hadj-Ali et al. [9] for MHEX as the fuel.

11

4.2. Pressure Traces

Figure 4a shows the pressure traces for selected experiments at $\phi = 1.0$, $P_C = 30$ bar. The three reactive pressure traces shown are at the low-temperature end of the NTC (blue, 700 K), one case with two-stage ignition (orange, 733 K), and one case near the high-temperature limit of the NTC region (green, 774 K). Also shown is the non-reactive pressure trace for the 700 K case (red). By comparing the 700 K pressure trace with the non-reactive pressure trace, it can be seen that there is substantial heat release prior to main ignition as measured by the deviation of the reactive pressure trace from the non-reactive trace. However, there is only one peak in the time derivative of the pressure, so no first-stage ignition delay is defined for this case. It can also be seen in Fig. 4a that the 775 K case shows some heat release prior to ignition, although again there is only one peak in the time derivative of the pressure. Furthermore, the heat release at 775 K appears to be more gradual than at the lowest temperature.
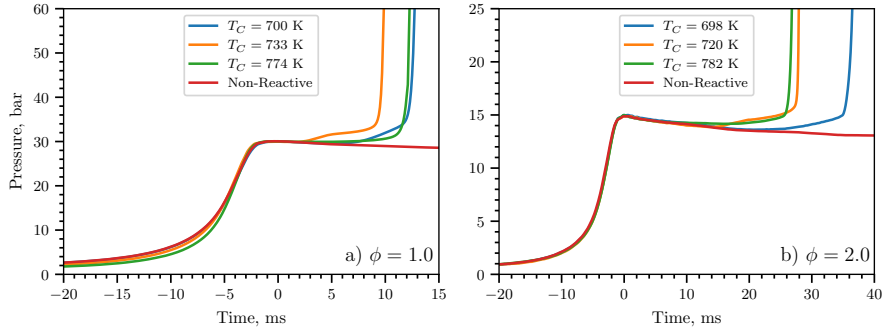
Figure 4: Selected pressure traces around the NTC region of ignition delay. a) $\phi = 1.0$ b) $\phi = 2.0$

A similar trend can be observed in Fig. 4b for $\phi = 2.0$ at $P_C = 15$ bar, where pressure traces at several points around the NTC region are plotted. As in Fig. 4a, the three reactive pressure traces shown are at the low-temperature end of the NTC (blue, 698 K), one case with two-stage ignition (orange, 720 K), and one case near the high-temperature limit of the NTC region (green, 782 K). Also shown is the non-reactive pressure trace for the 698 K case (red). As for

²⁴⁹ the $\phi = 1.0$ case, the pressure traces show significant heat release prior to the ²⁵⁰ overall ignition, as judged by deviation from the non-reactive case.

²⁵¹ 5. Computational Results

²⁵²   Figure 5 compares experimentally measured overall ignition delays with ig-
²⁵³ nition delays computed with the detailed model of Diévart et al. [15] (solid
²⁵⁴ lines). Figure 5a shows results at $P_C = 15\,\text{bar}$, while Fig. 5b shows results at
²⁵⁵ $P_C = 30\,\text{bar}$. Only some equivalence ratios are shown for each pressure con-
²⁵⁶ dition; data and simulated results are not shown for cases where the reactive
²⁵⁷ simulated temperature at the EOC deviated substantially from the non-reactive
²⁵⁸ temperature due to heat release during the compression stroke. Furthermore, it
²⁵⁹ is important to note that the model of Diévart et al. [15] was not validated for
²⁶⁰ MV ignition delays, only for extinction strain rates.

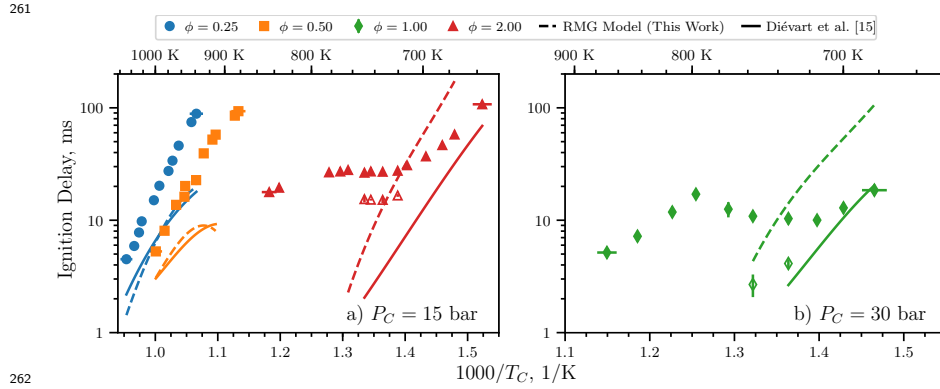²⁶¹

²⁶³   Figure 5: Comparison of experimental and simulated results. a) 15 bar; b) 30 bar

²⁶⁴   At 15 bar, the experimental ignition delays are under-predicted by the Diévart
²⁶⁵ et al. [15] model for the three equivalence ratios shown. For the $\phi = 0.25$ and
²⁶⁶ 0.5 conditions, the model appears to be predicting an NTC region of the igni-
²⁶⁷ tion delays as the temperature decreases, although such a trend is not observed
²⁶⁸ in the data. However, at $\phi = 2.0$, the model does not predict the presence of
²⁶⁹ an NTC region, although one is present in the experiments. Nonetheless, the

13

agreement seems to be improving as the temperature is decreased. Comparing the Diévart et al. [15] model to the data at 30 bar, we find a similar trend as the $\phi = 2.0$, $P_C = 15$ bar data. The model does not predict the NTC region found experimentally for the $\phi = 1.0$ experiments, but the agreement improves as the temperature decreases.

To elucidate the underlying reasons for the disagreement between the Diévart et al. [15] model and the data, we constructed an additional model using RMG (see Section 3.2). As can be seen in Fig. 5a, the agreement between the RMG model (dashed lines) and the experimental data is similar to the Diévart et al. [15] model for the 15 bar, $\phi = 0.25$ and 0.5 data. Moreover, the RMG model predicts a similar NTC region as temperature is decreasing. For the 15 bar, $\phi = 2.0$ data, the RMG model tends to over-predict the low-temperature ignition delays, and does not predict the NTC region found experimentally. As before, the trend at 30 bar, $\phi = 1.0$ is similar to the 15 bar, $\phi = 2.0$ data; the RMG model over-predicts the low-temperature ignition delays and does not predict the experimental NTC region.

It is clear that neither model is able to predict the ignition delays of MV particularly well. In addition to the poor agreement shown in Fig. 5, the simulations for $P_C = 15$ bar, $\phi = 1.0$ and $P_C = 30$ bar, $\phi = 0.25$, 0.5 and 2.0 showed substantial heat release during the compression stroke (i.e., the simulations are much too reactive), and so these conditions aren't compared in Fig. 5. We note again that the model by Diévart et al. [15] was validated for MV combustion only by comparison to flame extinction limits, so the disagreement is not wholly surprising.

In general, there could be three likely sources of error in the models: missing reaction pathways, incorrect values of the reaction rates, and incorrect values for thermodynamic properties of the species. We have noted in Section 3.2 that the RMG model has many more reactions than the Diévart et al. [15] model and the algorithm used in RMG considers a substantial number of the possible pathways. This reduces the possibility of missing reaction pathways affecting the model. Further detailed studies are required to ensure that the RMG model

14

includes all of the relevant reaction pathways, which are outside the scope of this work.

The second source of error may be incorrect reaction rate parameters, either because the rates are specified incorrectly in the model or because the rates are not well estimated by the typical analogy based-rules. It should be noted that errors of this type may affect the model generated by RMG—if the rates are not estimated correctly, reactions that are important in reality may not be included in the model. Determining the accuracy of the reaction rates used in the RMG and Diévart et al. [15] models requires further detailed studies of the models, which are also outside the scope of this work. Another, related, source of error could be incorrect estimation of the pressure dependence of the reaction rates, which may be particularly important for the isomerization reactions prevalent in low-temperature chemistry.

The third source of error may lie in the estimation of the thermodynamic properties of the species, particularly the fuel radicals. In the work of Diévart et al. [15], the program THERM [40] is used to estimate thermodynamic values using the group additivity method. In the RMG model constructed in this work, RMG itself estimates the thermodynamic properties of the molecules also using the group additivity method. Nonetheless, the two models have differing predictions of the thermodynamic properties of the species in the model, particularly the fuel and its radicals. The values of the heats of formation of the fuel and its H-atom abstraction radicals are shown in Table 3; the radicals are labeled according to the convention shown in Fig. 6.
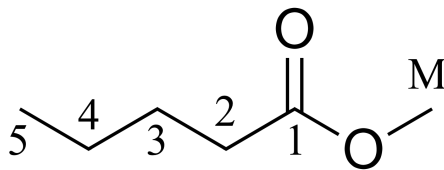
Figure 6: Structure of MV with carbon atoms labeled according to the convention used in Table 3 and Table 4

15

Table 3: Heats of formation of MV and its radicals, labeled according to the convention used in Fig. 6

Radical Site	Diévart et al. [15]		RMG Model	
	[kJ/mol]	[kcal/mol]	[kJ/mol]	[kcal/mol]
MV	−470.98	−112.57	−472.53	−112.94
2	−297.16	−71.02	−273.63	−65.40
3	−277.03	−66.21	−273.63	−65.40
4	−277.03	−66.21	−278.61	−66.59
5	−265.94	−63.56	−267.53	−63.94
M	−270.51	−64.65	−270.12	−64.56

Table 3 shows that the heats of formation of the fuel and radicals 3, 4, 5, and M are quite similar between the two mechanisms. However, the heat of formation of the second radical, the one closest to the methyl ester group, has a significantly lower heat of formation in the model by Diévart et al. [15] than in the RMG model. Note that it is expected that the second radical will be somewhat more stable than the other radicals, due to the influence of the methyl ester group on the adjacent carbon atom.

This difference in heats of formation affects the pathways that consume the fuel. By conducting a reaction pathway analysis to determine which radicals are formed from the breakdown of the fuel, we can analyze the proportion of each radical formed as the fuel breaks down during the autoignition process. The following analysis is conducted for a constant volume, adiabatic simulation with initial temperature and pressure of $700\,\text{K}$, $30\,\text{bar}$, and for the stoichiometric equivalence ratio. The rates of production of the species have been integrated until the time of $20\,\%$ fuel consumption. The results of this analysis are shown in Table 4 for the two models. The percentages shown in the Table 4 are the percent of the fuel consumed to form a particular fuel radical by all the reactions that can form that radical, and the radicals are labeled according to the convention in Fig. 6.

Table 4: Percent of MV consumed to form fuel radical species with a hydrogen atom missing at the location indicated in the first column and Fig. 6

Radical Site	Diévart et al. [15] [%]	RMG Model [%]	RMG switched [%]
2	29.2	12.5	11.0
3	17.5	12.2	11.1
4	17.5	50.6	56.6
5	9.5	3.9	4.3
M	26.3	20.8	16.9

At the relatively low temperature and high pressure condition of this analysis, all of the fuel is consumed by H-atom abstractions to form the fuel radicals shown. It can be seen that the two models have quite different distributions of products from the first H-abstraction reactions. The model of [15] predicts that H-abstraction from the second carbon is the most prevalent, while the RMG model predicts that the radical on the fourth carbon in the chain will be primarily formed. This is in line with the heats of formation in Table 3, where the most stable radical (i.e., the radical with the smallest heat of formation) is most likely to be formed in each model.

To further compare the models with each other, the NASA polynomials representing the thermodynamic properties of MV and the 5 fuel radicals from the model of Diévart et al. [15] and are used to replace the equivalent molecules in the RMG model. The results of a path analysis at the same condition as the other analysis is shown in Table 4 in the "RMG switched" column. This analysis shows that the radical on the fourth carbon atom is still the most prevalant, despite changing the heats of formation of the fuel and its radicals.

Taken together, these results show that the errors in a given model cannot be attributed to a single source. There is a strong interaction between the thermodynamics of the species and the kinetics of the reactions, requiring further detailed study of the methyl ester system to accurately predict the low temperature ignition delays of methyl valerate.

6. Conclusions

In this study, we have measured ignition delays for methyl valerate over a wide range of engine-relevant pressures, temperatures, and equivalence ratios. An NTC region of the ignition delay and two-stage ignition were recorded for pressures of 15 bar at $\phi = 2.0$ and 30 bar at $\phi = 1.0$. A detailed chemical kinetic model available in the literature was unable to reproduce the experimental results, so a new model was constructed using the Reaction Mechanism Generator software. Although the new model contains many more reactions than the literature model, it is still unable to predict the experimental ignition delays satisfactorily. Both models predict an NTC region of the ignition delay under conditions where none was found in the experiments, and fail to predict the NTC region of ignition delay that is present in the experiments. Possible reasons for the discrepancy include missing reaction pathways, incorrect rate estimates, and incorrect thermodynamic property estimates. Comparative analysis of the two models failed to identify a single source of the error, and further detailed studies are required to improve predictions of the ignition delay at these engine-relevant conditions.

References

[1] S. K. Hoekman, C. Robbins, Fuel Processing Technology 96 (2012) 237–249.

[2] J. Y. Lai, K. C. Lin, A. Violi, Progress in Energy and Combustion Science 37 (2011) 1–14.

[3] L. Coniglio, H. Bennadji, P. Glaude, O. Herbinet, F. Billaud, Progress in Energy and Combustion Science 39 (2013) 340–382.

[4] W. K. Metcalfe, S. Dooley, H. J. Curran, J. M. Simmie, A. M. El-Nahas, M. V. Navarro, The Journal of Physical Chemistry A 111 (2007) 4001–4014.

[5] S. M. Walton, M. S. Wooldridge, C. K. Westbrook, Proceedings of the Combustion Institute 32 (2009) 255–262.

[6] S. Dooley, H. J. Curran, J. M. Simmie, Combustion and Flame 153 (2008) 2–32. 16.

[7] B. Akih-Kumgeh, J. M. Bergthorson, Energy & Fuels 24 (2010) 2439–2448.

[8] B. Akih-Kumgeh, J. M. Bergthorson, Combustion and Flame 158 (2011) 1037–1048.

[9] K. Hadj-Ali, M. Crochet, G. Vanhove, M. Ribaucour, R. Minetti, Proceedings of the Combustion Institute 32 (2009) 239–246. 23.

[10] K. Kumar, C.-J. Sung, Combustion and Flame 171 (2016) 1–14.

[11] E. Fisher, W. J. Pitz, H. J. Curran, C. K. Westbrook, Proceedings of the Combustion Institute 28 (2000) 1579–1586. 10.

[12] O. Korobeinichev, I. Gerasimov, D. Knyazkov, A. Shmakov, T. Bolshova, N. Hansen, C. K. Westbrook, G. Dayma, B. Yang, Zeitschrift für Physikalische Chemie 229 (2015).

[13] A. M. Dmitriev, D. A. Knyazkov, T. A. Bolshova, A. G. Shmakov, O. P. Korobeinichev, Combustion and Flame 162 (2015) 1964–1975.

[14] C. Hayes, D. R. Burgess, Proceedings of the Combustion Institute 32 (2009) 263–270. 26.

[15] P. Diévart, S. H. Won, J. Gong, S. Dooley, Y. Ju, Proceedings of the Combustion Institute 34 (2013) 821–829.

[16] G. Mittal, C.-J. Sung, Combustion Science and Technology 179 (2007) 497–530.

[17] G. Mittal, C.-J. Sung, Combustion and Flame 145 (2006) 160–180.

[18] B. W. Weber, C.-J. Sung, in: S. Benthall, S. Rostrup (Eds.), Proceedings of the 15th Python in Science Conference, pp. 36–44.

[19] B. W. Weber, R. Fang, C.-J. Sung, UConnRCMPy, 2017.

19

[20] D. G. Goodwin, H. K. Moffat, R. L. Speth, Cantera: An Object-oriented Software Toolkit for Chemical Kinetics, Thermodynamics, and Transport Processes, 2017.

[21] S. van der Walt, S. C. Colbert, G. Varoquaux, Computing in Science & Engineering 13 (2011) 22–30.

[22] E. Jones, T. Oliphant, P. Peterson, others, SciPy: Open Source Scientific Tools for Python, 2001-.

[23] J. D. Hunter, Computing in Science & Engineering 9 (2007) 90–95.

[24] D. Lee, S. Hochgreb, Combustion and Flame 114 (1998) 531–545.

[25] J. Ortega, F. Espiau, J. Tojo, J. Canosa, A. Rodríguez, Journal of Chemical & Engineering Data 48 (2003) 1183–1190.

[26] A. G. Camacho, J. M. Moll, S. Canzonieri, M. A. Postigo, Journal of Chemical & Engineering Data 52 (2007) 871–875.

[27] R. M. Stephenson, S. Malanowski, D. Ambrose, Handbook of the Thermodynamics of Organic Compounds, Elsevier, New York, 1987.

[28] A. C. van Genderen, J. van Miltenburg, J. G. Blok, M. J. van Bommel, P. J. van Ekeren, G. J. van den Berg, H. A. Oonk, Fluid Phase Equilibria 202 (2002) 109–120.

[29] S. P. Verevkin, V. N. Emel'yanenko, Fluid Phase Equilibria 266 (2008) 64–75.

[30] E. E. Dames, A. S. Rosen, B. W. Weber, C. W. Gao, C.-J. Sung, W. H. Green, Combustion and Flame 168 (2016) 310–330.

[31] A. C. Hindmarsh, P. N. Brown, K. E. Grant, S. L. Lee, R. Serban, D. E. Shumaker, C. S. Woodward, ACM Transactions on Mathematical Software 31 (2005) 363–396.

[32] S. C. Chapra, R. P. Canale, Numerical Methods for Engineers, McGraw-Hill Higher Education, Boston, 6th ed edition, 2010.

[33] J. W. Allen, C. F. Goldsmith, W. H. Green, Physical Chemistry Chemical Physics 14 (2012) 1131–1155.

[34] B. W. Weber, C.-J. Sung, M. W. Renfro, Combustion and Flame 162 (2015) 2518–2528.

[35] B. W. Weber, K. E. Niemeyer, arXiv:1706.01987 [physics] (2017).

[36] G. Kukkadapu, K. Kumar, C.-J. Sung, M. Mehl, W. J. Pitz, Combustion and Flame 159 (2012) 3066–3078.

[37] M. Ribaucour, R. Minetti, L. R. Sochet, Symposium (International) on Combustion 27 (1998) 345–351.

[38] J. Bugler, K. P. Somers, E. J. Silke, H. J. Curran, The Journal of Physical Chemistry A 119 (2015) 7510–7527.

[39] K. A. Heufer, J. Bugler, H. J. Curran, Proceedings of the Combustion Institute 34 (2013) 511–518.

[40] E. R. Ritter, J. W. Bozzelli, International Journal of Chemical Kinetics 23 (1991) 767–778.